

# Impact of ground motion uncertainty evolution from post-earthquake data on building damage assessment

Earthquake Spectra

1–26

© The Author(s) 2024

Article reuse guidelines:

[sagepub.com/journals-permissions](https://sagepub.com/journals-permissions)

DOI: 10.1177/87552930241266808

[journals.sagepub.com/home/eqs](https://journals.sagepub.com/home/eqs)

Jorge-Mario Lozano, M.EERI , Iris Tien, M.EERI , Elliot Nichols, M.EERI, and J. David Frost, M.EERI

## Abstract

Accurate damage assessment after an earthquake is crucial for effective emergency response. Using ground motion information enables rapid building damage assessment when detailed damage data are unavailable. While uncertainty in earthquake parameters plays a significant role in the accuracy of rapid estimations, it is usually treated as a constant parameter rather than as a dynamic parameter that considers the amount of ground motion data collected that evolve over time. This work investigates the impact of incorporating evolving ground motion uncertainty in ground motion estimations from US Geological Survey's (USGS) ShakeMap on post-disaster damage assessments from two methodologies: the revised Thiel–Zsutty (TZR) model and Federal Emergency Management Agency's (FEMA) Hazus. Using data from the 2020 Indios earthquake in Puerto Rico and the 2014 Napa earthquake, we find that changes in uncertainty in estimates of peak ground acceleration reach 65% between early and late versions of the ShakeMap. We propose a process to integrate this evolution with the two damage assessment methodologies through a Monte Carlo simulation-based approach, demonstrating that it is critical to introduce dynamic ground motion uncertainty in the damage assessment process to avoid propagating unreliable measures. Both methodologies show that resulting damage estimates can be characterized by narrower distributions, indicative of reduced uncertainty and increased precision in damage estimates. For the TZR model, an improved estimate of post-disaster loss is achieved with narrower bounds in distributions of expected high scenario loss. For Hazus, the results show potential changes in the most probable damage state with an average change of 13% in the most probable damage state. The described methodology also demonstrates how uncertainty in the resulting damage state distributions can be reduced compared with the use of the current Hazus methodology.

---

School of Civil and Environmental Engineering, Georgia Institute of Technology, Atlanta, GA, USA

## Corresponding author:

Jorge-Mario Lozano, School of Civil and Environmental Engineering, Georgia Institute of Technology, Atlanta, GA 30332, USA.

Email: [jlozano32@gatech.edu](mailto:jlozano32@gatech.edu)

## Keywords

Damage assessment, post-disaster data, seismic risk, uncertainty quantification, building damage, disaster response, ShakeMap, Hazus, stochastic simulation, loss assessment

Date received: 7 October 2022; accepted: 6 June 2024

## Introduction

Rapidly assessing building damage is critical during the aftermath of a disaster. For example, emergency managers require situational awareness of damage to manage resources, personnel, and evacuations. Having a detailed description of damage across an affected area improves the prioritization of assets to facilitate post-disaster recovery. Thus, having an effective and accurate protocol for damage assessment is central to enhancing the disaster resilience of a region.

Accurate damage assessment combines multiple technologies and approaches, some of which require substantial time to capture aspects of the data in the field. The resulting data sets often also require significant processing before they can be effectively used in post-disaster decision-making. One approach that overcomes these obstacles is to use early ground motion data to rapidly estimate building damage. For seismic events, one of the first data sets available is US Geological Survey's (USGS) ShakeMap, a spatial representation of ground motion parameters and earthquake intensity (Wald et al., 2005). The ShakeMap is usually published 20 min after the event and is frequently updated as new data are collected (Wald et al., 2022). To transform the data from the ShakeMap into estimates of building damage, models are used that combine data from the severity of the earthquake (i.e., the ShakeMap), local site conditions (e.g., soil type), and information about the built environment to perform damage assessments. These empirical models that merge earthquake data are useful for response activities during the first week after an earthquake, when there is little information about damage in the field. FEMA's Hazus, for instance, is one of the tools capable of merging these various data sets (Kircher et al., 2006).

The outcomes of these damage estimations can be subject to high uncertainty given the lack of data and the complexity of nature's processes (Handmer, 2002). This includes the ground motion uncertainty, that is, the uncertainty on the intensity of the ground motion at a specific location and uncertainty in structural responses to a given loading. To model these uncertainties, fragility curves are commonly used, which represent the probability of reaching or exceeding a certain level of damage given a ground motion parameter (e.g., peak ground acceleration (PGA)) (Baker et al., 2021). In damage assessment methodologies such as Hazus, the uncertainty in fragility curves is represented by a parameter  $\beta$  that accounts for all uncertainty sources including seismic, structural, and site-specific sources (Porter et al., 2002).

While uncertainty plays a significant role in the accuracy of rapid post-disaster damage assessment, particularly for seismic events, fragility curves typically consider ground motion uncertainty as a constant value that depends only on previous events and empirical measures (Porter, 2010; Thiel Zsutty, 1987). In other words, even when more data are collected and estimations improve in the ShakeMap, most methodologies do not update the ground motion uncertainty to estimate the damage. Figure 1 illustrates how damage assessments evolve over time after an earthquake event. Estimated performance of a structure or system is shown as a solid line. Early rapid damage estimations are subject to higher uncertainty (green shaded area), and as more detailed damage data are collected,

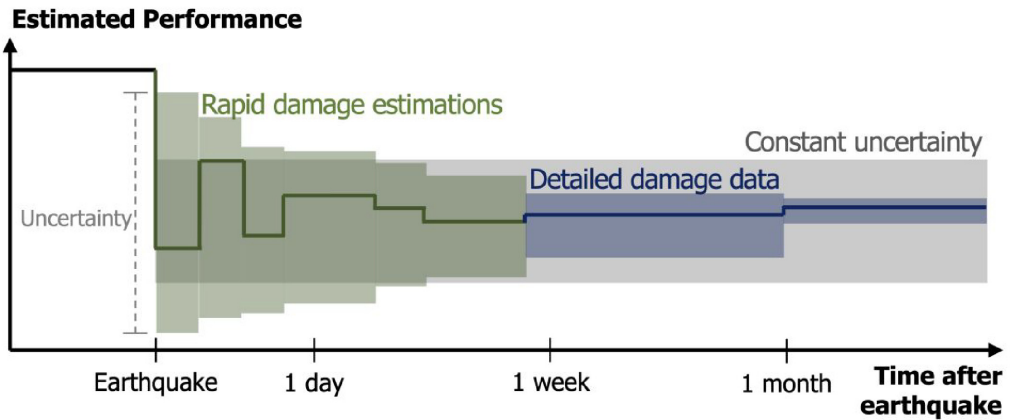


**Figure 1.** Evolution of a system's damage comparing dynamic and constant uncertainty.

the uncertainty decreases (blue shaded area). In contrast is the constant uncertainty (gray shaded area), which is time invariant. Using constant ground motion uncertainty values resulting in constant structural performance assessment uncertainty can underestimate the uncertainty in the early stages after an earthquake and overestimate it in later stages when detailed damage data are available. This misrepresentation of ground motion uncertainty leads to inaccurate estimations of damage and loss, particularly for metrics highly dependent on ground motion parameters, such as estimations of economic impacts, which are critical for emergency managers and insurance companies to allocate necessary funds to respond to an earthquake (Bhattacharjee et al., 2022; Doggett and Fobert, 2013).

Ground motion uncertainty has been previously identified to affect the results of damage assessment (Bommer and Crowley, 2006; Ioannou et al., 2015). Nonetheless, previous works in improving estimates of damage after earthquakes have mostly focused on addressing structural response uncertainty using fragility curves and stochastic modeling in specific structures (Celarec and Dolšek, 2013; Liel et al., 2009; Rota et al., 2014; Vamvatsikos and Fragiadakis, 2009). Some works have highlighted the need for improving the modeling of ground motion uncertainty in building damage assessment (Abrahamson and Bommer, 2005 and Borgonovo et al., 2013) but, as of now, there is no quantification of these impacts in damage assessment using real ground motion data. For the ShakeMap, Kircher (2002) recognized the need to decrease the uncertainty in the Hazus methodology when input seismic data come from a ShakeMap. However, even when this modification improves the values of uncertainty in the damage estimations, this modification still treats ground motion uncertainty as a constant value that does not change throughout the post-earthquake period.

With this gap in incorporating dynamically evolving ground motion uncertainty in damage assessment, this article quantifies the effect of incorporating the evolution of ground motion uncertainty, namely uncertainty in the PGA, in damage assessment methodologies. For this purpose, we consider ground motion data from two events: the Indios 2020 earthquake in Puerto Rico and the South Napa 2014 earthquake in California. In addition to the ShakeMap analysis of these events, we propose a methodology to quantify the impact of the evolution of ground motion uncertainty in two widely used approaches for building damage assessment: the revised Thiel–Zsutty (TZR) model and Hazus loss methodology. The proposed methodology considers damage from ground motion and not from ground failure (e.g., fault rupture, lateral spreading, liquefaction, and landslides).

The remainder of the article includes a description of uncertainty parameters in the ShakeMap, followed by a quantification of the evolution of earthquake parameters in evolving versions of the ShakeMap for both earthquake events. Then, a description of the two damage assessment methodologies is described, along with the proposed process to explicitly incorporate evolving ground motion uncertainty into these methodologies. The resulting damage state distributions from implementing the proposed approach are compared with those from current methods to demonstrate the effect of including dynamically evolving ground motion uncertainty information in the estimation outcomes of post-disaster building damage states.

## Uncertainty in the ShakeMap

A ShakeMap provides information on multiple earthquake parameters to quantify the severity of an earthquake. This data set is the primary data set used for rapid post-earthquake analysis, given that it is consistently published for all significant earthquakes and relies on large networks of seismometers across the world (Wald et al., 2005). The ShakeMap is based on information from three sources: ground motion recordings from seismometers, ground motion models (GMMs), and survey “Did you feel it?” (DYFI) responses from people who experienced the earthquake. Records from seismometers are processed to determine the epicenter by interpolating the values of the earthquake parameters (Worden et al., 2018). Then, a combination of GMMs is chosen to model the attenuation of ground motions around the epicenter. Finally, DYFI data improve the reliability of intensity measures with questions related to observed damage and people’s experiences (Atkinson and Wald, 2007).

The first version of the ShakeMap is typically released 20 min after an event with significant uncertainties, given the use of only part of the seismometer network, suitability of the initially chosen GMMs, and inherent uncertainties in the responses of the DYFI surveys (Wald et al., 2008). These uncertainties are quantified and included in each version of the ShakeMap, where each parameter is modeled as a lognormal distribution characterized by its two parameters, median and lognormal standard deviation. For example, the cumulative distribution function (CDF) of the PGA in the ShakeMap is presented in Equation 1.

$$P(PGA \leq x | PGA_{med}, \beta_d) = \Phi \left[ \frac{1}{\beta_d} \ln \frac{x}{PGA_{med}} \right], \quad (1)$$

where  $\Phi$  is the standard normal CDF,  $PGA_{med}$  is the median PGA reported in the ShakeMap, and  $\beta_d$  is the lognormal standard deviation (uncertainty parameter) reported on the ShakeMap. This notation is extended to damage assessment methodologies such as Hazus where  $\beta_d$  indicates the uncertainty coming from the hazard demand.

Each data source provides information on the uncertainty of the earthquake parameters (Wald et al., 2008). First is the influence of any proximal seismometer recordings. Second is the uncertainty from the GMMs, which is higher near the epicenter due to modeling complexities. Third, especially in areas with low seismometer density, are DYFI data points, where an increased number of survey responses decrease the uncertainty in the earthquake parameters. Having multiple versions of the ShakeMap introduces a dynamic evolution component to estimating these earthquake parameters. This evolution is examined more closely in the following section.

## Evolution of seismic hazard parameters

This section illustrates the evolution of earthquake parameters using data from two events: the Mw 6.4 Indios, Puerto Rico, earthquake in 2020, and the Mw 6.0 Napa, CA, earthquake in 2014 (USGS, 2014, 2020). These events are selected as recent events with varying instrumentation and data availability characteristics to show the generalizability of the approach across seismic events. In addition, both events have similar magnitudes and allow for comparisons across events of different instrumentation. ShakeMap data were downloaded using the Comprehensive Catalog (ComCat) from the Advanced National Seismic System (ANSS). This section describes the data sources from each event. It then discusses the spatial distribution in various versions of the ShakeMap per event and the evolution of PGA distributions at specific locations with varying distances from the epicenter and uncertainty levels.

### Data sources by event

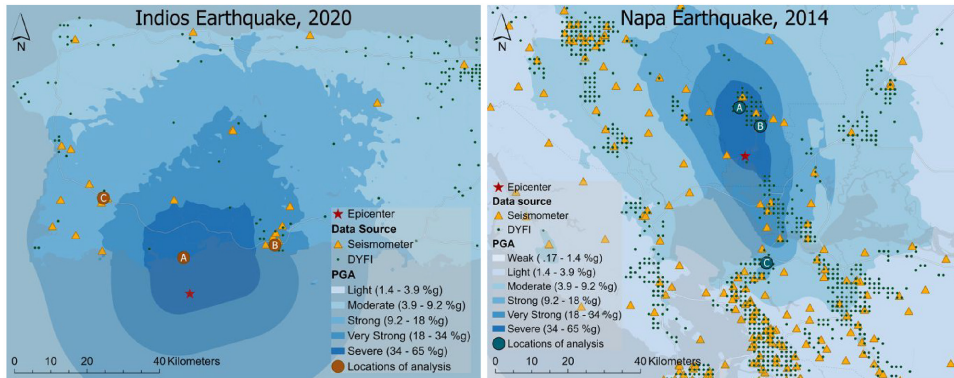
Figure 2 illustrates the data sources for both events, estimated epicenter, and the distribution of PGA across the area. Individual seismometer locations are shown, and the DYFI data are shown to the nearest 1 km-by-1 km grid point. Median PGA distribution from the final version of the ShakeMap is shown (version 10 for Indios, version 33 for Napa). Each map also includes the three locations of analysis for each event that will be used at the end of this section. Key properties of the two earthquakes are shown in Table 1.

Figure 2 and Table 1 highlight differences in data sources by event. For the number of seismometers, there are only 31 used in Indios compared with 966 in Napa. The number of DYFI data points also differs significantly with 1610 in Indios compared with 16,679 in Napa. Multiple factors contribute to the difference in DYFI responses such as differences in Internet infrastructure and awareness of earthquake technologies. The availability of data across different sources influences the resulting ground motion parameter uncertainty estimates for each event.

### Evolving PGA distribution parameters across ShakeMap versions

Every new version of the ShakeMap augments or changes information from the multiple data sources. In this way, the earthquake parameters evolve as they are continually updated. Figures 3 and 4 illustrate the evolution of the median PGA ( $PGA_{med}$ ) and its log-normal standard deviation ( $\log \sigma_{PGA}$  or  $\sigma_{PGA}$  for simplicity) for both events. In Figure 3 for the Indios earthquake, versions 1, 3, and 8 are shown. In Figure 4 for the Napa earthquake, versions 1, 13, and 27 are shown. These versions are chosen as the initial ShakeMap (V1), a middle version with more seismometers included, and the version after the finite fault model (FFM) is included. The inclusion of the FFM provides information about the size and shape of the fault rupture, which improves the modeling of the distribution of ground motion intensity parameters.

From Figures 3 and 4, the changes in the estimated distribution of the PGA median are visible. For the Indios earthquake, the  $PGA_{med}$  has two main changes across the versions. First, from V1 to V3, the location of the epicenter shifts to the east. Second, from V3 to V8, the rupture changes from a point source to a rectangular one. In the Napa earthquake, from V1 to V13, there was a clear increase in  $PGA_{med}$  in regions near the epicenter. Then, from V13 to V27, the rupture is no longer modeled as a point but as a line.



**Figure 2.** Data sources and peak ground acceleration from final version of the ShakeMap for the Indios earthquake (left) and the Napa earthquake (right).

**Table 1.** Summary properties for the Indios and Napa earthquakes

Event	Indios	Napa
Location	17.869 N 66.827 W Depth: 9 km	38.22 N 122.31 W Depth: 11 km
Origin time (local)	2020-01-07 04:24:25	2014-08-24 03:20:44
Magnitude (Mw)	6.4	6.0
ShakeMap versions	10	33
Seismometers	31	966
Total DYFI responses	1610	16,679
Ground motion model (GMM)	Abrahamson et al. (2014), Boore et al. (2014), Campbell and Bozorgnia (2014), Chiou and Youngs (2014)	Boore and Atkinson (2008)

For the lognormal standard deviation  $\sigma_{PGA}$ , there is also a clear evolution for both events. For the Indios earthquake, given the fewer number of seismometers,  $\sigma_{PGA}$  in V1 and V3 is dominated by the parameters of the GMM considered in each version. As a result, the highest ground motion uncertainty is at the epicenter and it decreases radially with distance from this location (shown as a large dark purple circle). As more seismometers and DYFI data are included from V1 to V3, clusters of lower  $\sigma_{PGA}$  appear as pink spots. Finally, after the FFM is added in V8, the  $\sigma_{PGA}$  no longer depends on the GMM because the ShakeMap algorithm assumes complete knowledge of the rupture geometry (Worden, 2016). Instead,  $\sigma_{PGA}$  in V8 depends on the location of seismometers and DYFI responses (shown as light-yellow spots).

The dynamics of  $\sigma_{PGA}$  are different for the Napa earthquake. The density of seismometers makes  $\sigma_{PGA}$  relatively low for the initial versions. In V1, for instance, low  $\sigma_{PGA}$  values are observed close to the sensors and increase with distance radially away from each sensor. As more sensors are included in the analysis,  $\sigma_{PGA}$  decreases, shown on the map as the values become lighter in color. This highlights the importance of having increased data from seismometers. Additional visualizations of the ShakeMap parameters evolution can be found at <https://arcg.is/14uiWHO>, including dynamic and interactive maps.

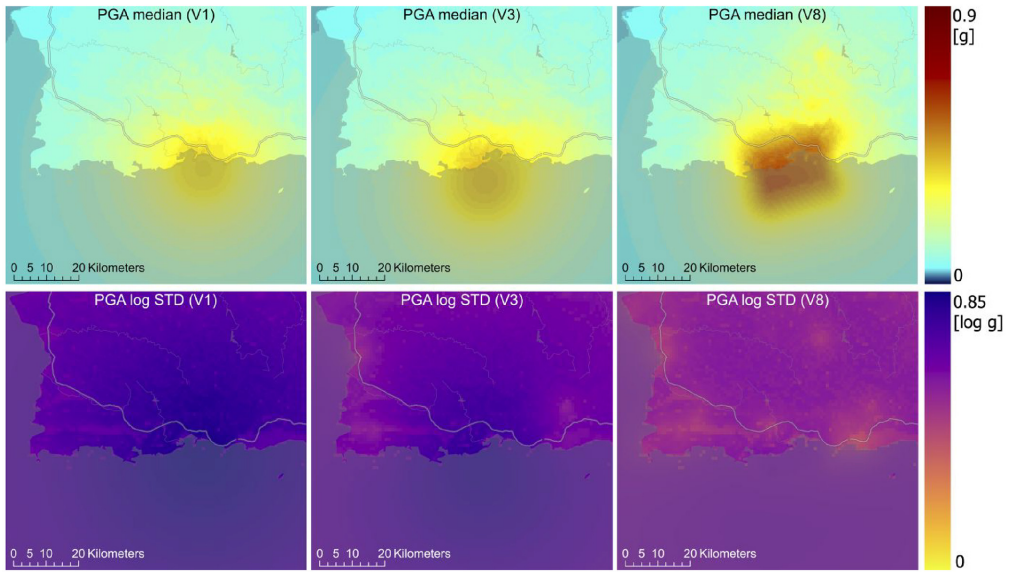


**Figure 3.** ShakeMap evolution for the Indios earthquake (versions 1, 3, and 8).

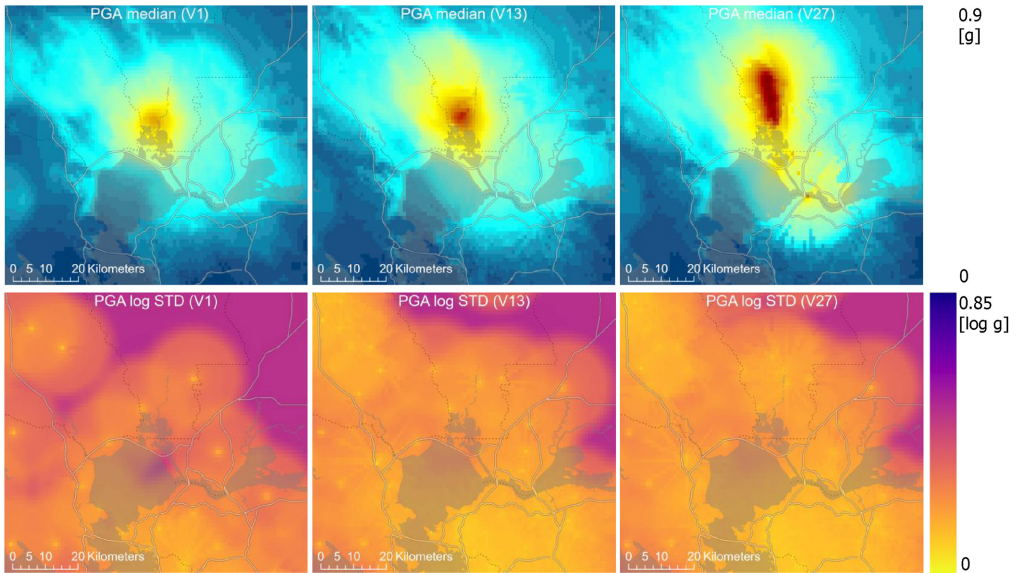


**Figure 4.** ShakeMap evolution for the Napa earthquake (versions 1, 13, and 27).

### *Varying distance from epicenter and uncertainty level*

There is significant spatial variability of ground motion parameters across an area impacted by an earthquake event. Therefore, this section analyzes the evolution of  $PGA_{med}$  and  $\sigma_{PGA}$  across three locations of varying characteristics:

1. Coordinate with the highest  $PGA_{med}$  post-FFM data,
2. Coordinate at a cluster of low  $\sigma_{PGA}$  near the epicenter, and
3. Coordinate at a cluster of low  $\sigma_{PGA}$  far from the epicenter.

In addition to varying distance from the epicenter and uncertainty level, the level of shaking (i.e.,  $PGA_{med}$ ) varies at each location, with location A being the highest (post-FFM data) and location C being the lowest. These three locations for each event are also those used to illustrate the impacts of integrating evolving ground motion uncertainty into the Hazus loss methodology described later in this article. Table 2 describes the parameters for all locations and events, including information for two ShakeMap versions: pre-FFM, which is V1 for both events, and post-FFM (V8 in Indios and V27 in Napa). Note that  $\sigma_{PGA}$  also represents the value of seismic hazard uncertainty  $\beta_D$  (see Equation 1), which will be used in later sections.

To better visualize the changes in these parameters across the ShakeMap versions published in the time after the event, Figure 5 illustrates the evolution of  $PGA_{med}$  (solid line) and the bounds of the lognormal distribution (shaded area) for the three locations of analysis of both events (Indios in orange and Napa in blue). The bounds shown are one standard deviation away from the mean, and each circle indicates a new version of the ShakeMap.

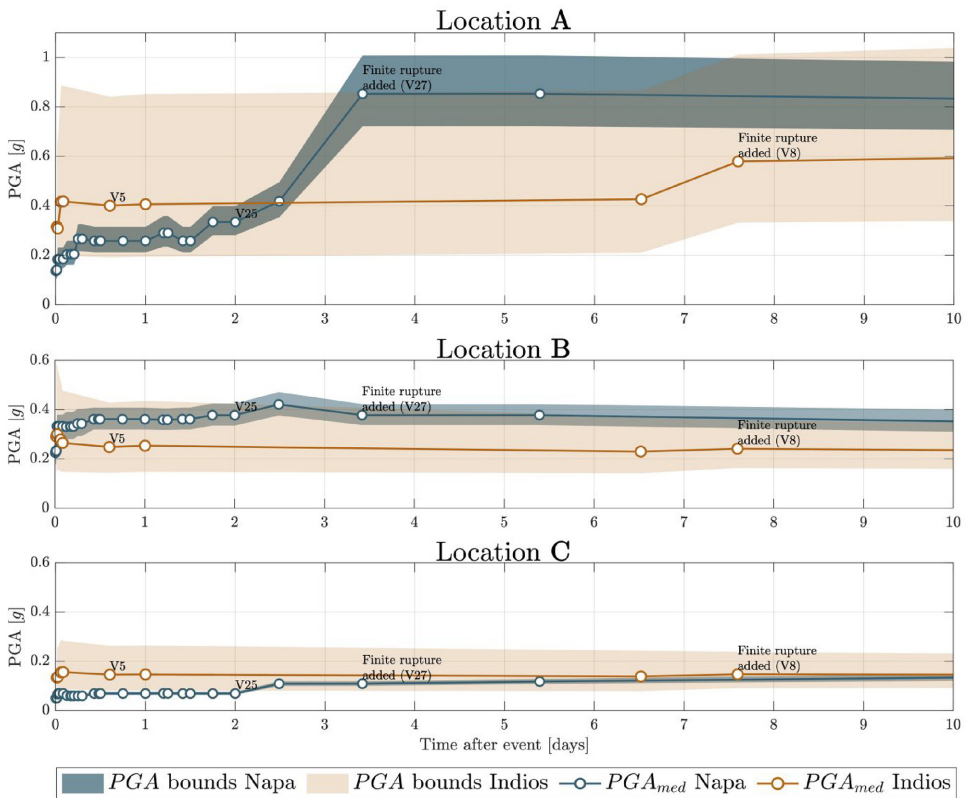
From Figure 5, the main observations are as follows:

1. There is a significant difference in the number of versions published. While after 2 days, there were 25 versions of the ShakeMap published for the Napa earthquake, there were only six versions for Indios. This is due to the differing data sources available, and the possibility to frequently update the ShakeMap with data from more sensors and DYFI responses for the Napa event. In addition, the Indios earthquake had an offshore epicenter, making it more challenging to record.
2. The PGA distribution is subject to large changes during the first days after the event as data from more seismometers and DYFI points are incorporated into the ShakeMap and the distribution is updated to account for the new data that are collected. In all locations of the Napa earthquake,  $PGA_{med}$  was initially underestimated. When comparing pre- and post-FFM, the increase in  $PGA_{med}$  was 507% in location A, 65% in location B, and 120% in location C.  $PGA_{med}$  from Indios is more stable, not as a result of less uncertainty (as shown by the bounds), but from the lack of additional data that are available to add. For both events,  $\sigma_{PGA}$  does change, decreasing a maximum of 44% for Indios and 65% for Napa.
3. FFM inclusion is faster for the Napa compared with Indios earthquake (3.4 vs 7.6 days). Similar to the number of versions, this difference results from sensor availability and the difficulties of modeling offshore earthquakes with high accuracy.
4. Changes in the PGA distribution post-FFM are minimal. Following the inclusion of the FFM,  $PGA_{med}$  varies less than 0.05 g and  $\sigma_{PGA}$  less than 0.05 log g in both events.
5. A decrease in  $\sigma_{PGA}$  does not always result in narrower bounds. Analyzing the shapes of PGA bounds reveals the compound effect of  $PGA_{med}$  and  $\sigma_{PGA}$ , especially in the lognormal distribution since it is in the logarithmic space, in which equal standard deviations do not result in the same shape of the distribution if the values of the median are different. This behavior is evident in Napa's location A,



**Table 2.** PGA median and lognormal standard deviation for locations of analysis

Parameter	Indios			Napa		
	A	B	C	A	B	C
Location						
Longitude	66.8423°W	66.6165°W	67.0409°W	122.3262°W	122.2746°W	122.2592°W
Latitude	17.9534°N	17.9827°N	18.0938°N	38.3086°N	38.2725°N	38.0062°N
Distance to epicenter (km)	10.03	26.95	35.49	13.38	9.16	30.12
Pre-FFM	PGA <sub>med</sub> (g)	0.32	0.29	0.13	0.14	0.23
	$\sigma_{PGA}$ ( $\beta_D$ )	0.78	0.70	0.67	0.27	0.25
Post-FFM	PGA <sub>med</sub> (g)	0.58	0.24	0.15	0.85	0.38
	$\sigma_{PGA}$ ( $\beta_D$ )	0.55	0.39	0.48	0.16	0.11

**Figure 5.** PGA median and bounds ( $\pm$  one standard deviation) for the three locations of analysis.

where there is a decrease in  $\sigma_{PGA}$  post-FFM (0.27 in V1 vs 0.16 in V27). However, given that PGA<sub>med</sub> increased from 0.14 to 0.85 g, the latter distribution is much wider even when  $\sigma_{PGA}$  decreased.

- The PGA distribution is highly dependent on data sources and the inclusion of FFM. As a result of all previous observations, the bounds on the PGA distributions from Napa are narrower than those from Indios. In addition, for the Indios earthquake, the inclusion of FFM has a relatively larger effect in decreasing the  $\sigma_{PGA}$  because the high density of data points in Napa better captures the rupture shape in the first days after the event.

From Figures 3 to 5, there is a clear evolution in estimated earthquake parameters throughout the post-earthquake period. Both the spatial and temporal distributions of PGA show changes in median and standard deviation, and in particular, changes in ground motion uncertainty ( $\sigma_{\text{PGA}}$ ) are highly dependent on the data sources of the event and if the FFM has been included or not. The next section quantifies the impact of these changes in the results of damage assessment methodologies.

## Impact on post-disaster damage assessment

This section investigates the impact of including the evolution of earthquake parameters from the ShakeMap in the results of two damage assessment methodologies: the revised TZR model and FEMA's Hazus. These methods are selected as two widely used damage and loss assessment methodologies. They also account for seismic parameter uncertainty differently, enabling illustration of the incorporation and impact of ground motion hazard uncertainty evolution information in two different approaches.

### *TZR model*

The revised TZR model is a methodology that estimates the probability density function (PDF) of loss based on the earthquake damageability of buildings (Thiel and Zsutty, 2017). The damage metric is called the scenario expected loss (SEL) and is calculated based on three main factors:

1. Intensity of the ground motion,
2. Site-specific characteristics, and
3. Uncertainty factor.

The TZR model is widely used by insurance and financial companies for pre- and post-disaster estimation of expected economic losses. Its simplicity of merging hazard parameters and building characteristics makes it useful for a broad and rapid estimate of expected losses after an earthquake. A description of the TZR methodology, how ground motion uncertainty is incorporated into the loss assessment, and the resulting impact of including ground motion uncertainty in the estimations of post-disaster loss are provided below.

### *TZR methodology*

The TZR model consists of two steps: calculating a damage rate (Equation 2) and constructing a beta probability distribution for SEL (Equations 3 to 7). The damage rate is calculated as:

$$p = 0.651b m s a^{0.606}; p \in (0, 1) \quad (2)$$

where  $p$  is the damage rate, representing the ratio between the repair and replacement cost (i.e.,  $p = 1$  when the repair costs equal the replacement costs);  $b$  is a factor representing the building vulnerability;  $m$  is a factor representing the spectral matching (or liquefaction susceptibility);  $s$  is a factor indicating soil type; and  $a$  is the PGA. For detailed descriptions and values per structural system, refer to the work by Thiel and Zsutty (2017). The value of the damage rate  $p$  from Equation 2 is then used to determine the parameters of the

probability distribution of SEL, where SEL is modeled as a beta distribution with parameters  $\lambda$  and  $\nu$ .

$$\mu = 0.41p^3 - 0.296p^2 + 0.857p - 0.014 \quad (3)$$

$$\sigma = \epsilon(1.853p - 6.825p^2 + 13.65p^3 - 13.11p^4 + 4.51p^5) \quad (4)$$

$$\lambda = \frac{(1 - \mu)\mu^2}{\sigma^2} - \mu \quad (5)$$

$$\nu = \frac{(1 - \mu)}{\mu} \lambda \quad (6)$$

$$SEL(x) \sim Beta(x, \lambda, \nu) \forall x \in [0, 1] \quad (7)$$

An SEL value of 1 indicates complete damage and corresponding loss; a value of 0 indicates zero damage and no loss. Note that the standard deviation  $\sigma$  of the distribution of SEL includes a parameter  $\epsilon$ , which represents the uncertainty factor of the problem and characterizes the uncertainty in the results.

*Integrating ground motion uncertainty: methods and results.* To propagate the ground motion uncertainty to the damage distribution in the TZR model, the uncertainty in the PGA from the ShakeMap ( $\sigma_{PGA}$ ) is introduced through parameter  $a$  in Equation 2. Rather than treating it as a constant deterministic value, parameter  $a$  becomes a lognormal random variable with time-evolving median  $PGA_{med}$  and lognormal standard deviation  $\sigma_{PGA}$ . Having  $a$  as a random variable transforms the SEL beta distribution parameters ( $\lambda, \nu$ ) to random variables given their dependency. To illustrate the changes in the SEL distribution by incorporating the dynamically evolving seismic hazard parameters, three values of the PGA distribution are used: the median  $PGA_{med}$  and the two PGA values at  $\pm$  one standard deviation from the median.

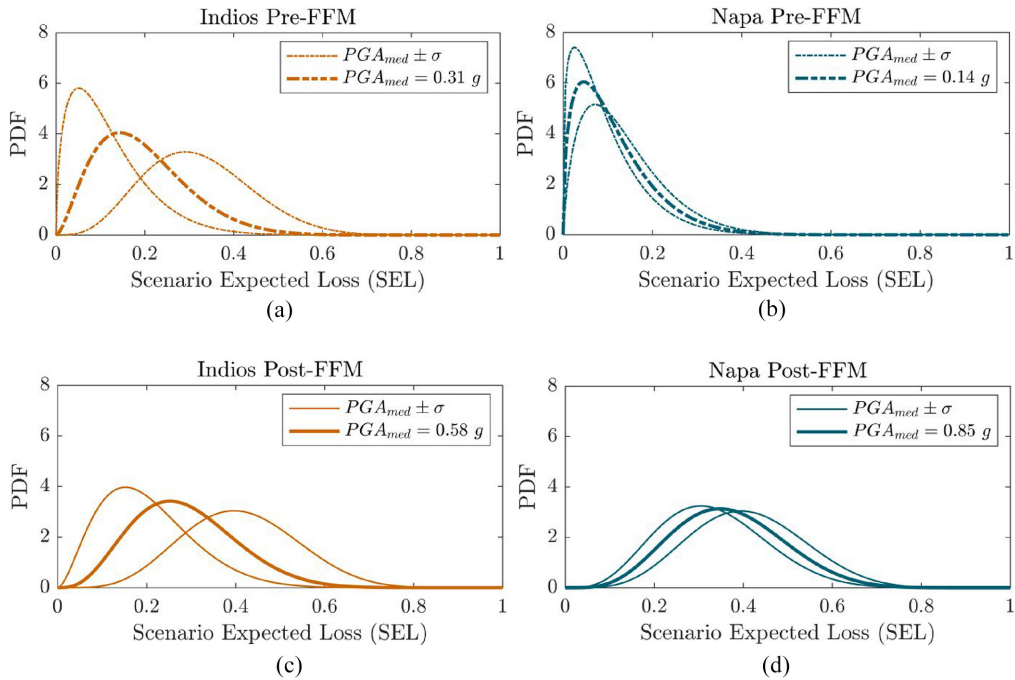
Using the parameters for an unreinforced masonry building with an interior frame, as shown in Table 3, and the ShakeMap of location A at both events, Figure 6 shows how the SEL distribution changes with the varying parameters. Pre-FFM and post-FFM indicate the resulting SEL distributions before and after a FFM is included, respectively. Changes between distributions at the other locations show similar results and are not included here.

For both events, the increase in  $PGA_{med}$  from pre- to post-FFM results in a shift of the distribution to the right after FFM is added, increasing the probability of having greater damage and correspondingly higher loss levels. In terms of uncertainty, the effect of  $\sigma_{PGA}$  in SEL is evident in the change in the spread of the distributions once FFM information is included.

In addition to assessing the overall distribution of SEL, a common use of the TZR model is calculating the probability that SEL is higher than 0.2. Financial institutions in particular use this model to estimate the economic impacts of an earthquake. Table 4 quantifies these values, reporting the probabilities pre- and post-FFM for both events. The mean SEL values given a value of PGA are provided, and the  $P(SEL > 0.2)$  is summarized. Also provided are the ranges at  $\pm$  one standard deviation of  $PGA_{med}$  for each case.

**Table 3.** TZR model parameters

Parameter	Value
$b$	0.64
$m$	1
$s$	1.25
$E$	0.5

**Figure 6.** SEL distribution at location A of Indios earthquake (a) VI and (b) V8, and Napa earthquake (c) VI and (d) V27.**Table 4.** Scenario loss distributions using the TZR model for location A in both events

Event	Finite fault data	$PGA_{med}$ (g)	$\sigma_{PGA}$ ( $\beta_D$ )	Mean (SEL—PGA)			P(SEL > 0.2) ( $\mu - \sigma, \mu, \mu + \sigma$ )
				$PGA_{med} - \sigma$	$PGA_{med}$	$PGA_{med} + \sigma$	
Indios	Pre	0.32	0.78	0.12	0.19	0.32	(0.16, 0.42, 0.83)
	Post	0.58	0.55	0.20	0.29	0.41	(0.45, 0.75, 0.96)
Napa	Pre	0.14	0.27	0.09	0.11	0.13	(0.10, 0.14, 0.21)
	Post	0.85	0.16	0.33	0.36	0.41	(0.86, 0.92, 0.96)

In Table 4, the uncertainty in the estimated SEL is dependent on the amount of information available for an earthquake event. The mean values of the SEL in Indios post-FFM range from 0.20 to 0.41, whereas the effect of having 3.4 times lower PGA

uncertainty (comparing  $\sigma_{\text{PGA}}$  values) makes the SEL distributions vary from 0.33 to 0.41 post-FFM for the Napa earthquake (Figure 6d). The effect of having more information, for example, more seismometers, results in a narrower SEL probability distribution, which is also shown in Figure 6b and d, decreasing the uncertainty in SEL and improving the estimations of damage loss.

Similar results are seen in the quantification of  $P(\text{SEL} > 0.2)$ , which for the Indios earthquake post-FFM ranges from 0.45 to 0.96, a large range that indicates imprecise estimates of damage due to the event. On the contrary, having a large network of sensors for the Napa earthquake results in a smaller estimation range of  $P(\text{SEL} > 0.2)$  from 0.86 to 0.96 after FFM is added. Still, even with less information for the Indios earthquake, an improvement in estimated SEL, measured by decreased  $\sigma_{\text{PGA}}$  when accounting for evolving PGA parameters between the pre- and post-FFM versions of the ShakeMap, is observed. The  $\pm$  one standard deviation range of  $P(\text{SEL} > 0.2)$  decreases from 0.67 to 0.51, indicating a smaller range in the estimate post-FFM compared with pre-FFM information. The range of the mean SEL value for the Napa earthquake increases for the post-FFM compared with pre-FFM estimate. This is due to the increase in  $\text{PGA}_{\text{med}}$  and concomitant increase in uncertainty for the higher intensity earthquake event. However, the post-FFM information result is considered to be a more accurate assessment of SEL as the most up-to-date seismic hazard information is included in the calculation.

The TZR model currently accounts for fragility uncertainty and mainly focuses on structural parameters. The results in this section show that in addition to structural response uncertainty, including ground motion uncertainty that considers the location of the event, its intensity, and its data sources, can result in improved uncertainty quantification and loss scenarios that better represent the total uncertainty in the building damage.

### *Hazus loss assessment*

The Hazus earthquake loss methodology is one of the most widely used tools for post-disaster building damage assessment (Kircher et al., 2006). Developed by FEMA, this software assesses direct physical damage to infrastructure (e.g., buildings, critical facilities, and utility systems) based on ground motion data. In addition to damage assessment, Hazus complements its results by estimating economic losses, casualties, and induced physical damage (i.e., debris and fires) (FEMA, 2020). Hazus can also be used for pre-disaster mitigation by analyzing potential outcomes from multiple hazard scenarios. In the context of this article, we focus on the products used immediately after an earthquake, that is, those that provide damage estimations based on ShakeMap ground motion data.

*Hazus methodology.* To describe how to incorporate ground motion hazard uncertainty information into updates of damage assessment in Hazus, it is necessary to understand how hazard data are used in the methodology. The process from hazard information to damage assessment is summarized in four steps:

1. Computing the demand spectrum. This curve is calculated using three parameters from the ShakeMap: PGA, pseudo-spectral acceleration at 0.3 s ( $\text{PSA}_{0.3 \text{ s}}$ ), and pseudo-spectral acceleration at 1 s ( $\text{PSA}_{1 \text{ s}}$ ).
2. Computing the building capacity curve. The structural parameters needed to build the curve can be found in the Hazus manual (FEMA, 2020).

3. Finding the performance point. This point is located at the expected spectral displacement,  $S_d$ , of the building, which is found by joining the reduced demand spectrum (a variation of the curve from step 1) and the capacity curve from step 2. The reduced demand spectrum is computed from the demand spectrum of step 1 and following the procedure in FEMA P-155 Section 5.3.5 (FEMA, 2015).
4. Determining damage state,  $ds$ , exceedance probabilities with fragility curves. These curves quantify the probability of the building exceeding each damage state for a given spectral displacement  $S_d$ . Hazus considers five damage states (i.e., None, Slight, Moderate, Extensive, and Complete). Definitions of every damage state per structural system can be found by FEMA (2020). The probabilities from these CDFs can then be used to calculate the probability of the building being in each damage state  $ds$ .

In summary, the Hazus damage assessment tool uses ShakeMap ground motion data combined with building parameter information to generate a distribution of the probabilities of a building being in each damage state.

In this procedure, step 4 accounts for the uncertainty in the random variables. The use of fragility curves helps to model the connection between ground motion and structural uncertainty. In Hazus, as with seismic variables from the ShakeMap, building fragility curves are modeled as cumulative lognormal distributions, as shown in Equation 8.

$$P[ds|S_d] = \Phi \left[ \frac{1}{\beta_{ds}} \ln \left( \frac{S_d}{\overline{S_{d,ds}}} \right) \right] \quad (8)$$

where  $\overline{S_{d,ds}}$  is the median displacement threshold of each damage state,  $\beta_{ds}$  is the total uncertainty on damage state  $ds$ , and  $\Phi()$  is the standard normal CDF. The uncertainty on each damage state  $\beta_{ds}$  is represented by:

$$\beta_{ds} = \sqrt{\text{CONV}(\beta_D, \beta_C, \overline{S_{d,ds}})^2 + \beta_T^2} \quad (9)$$

where  $\beta_D$  is the ground motion uncertainty (i.e., from the ShakeMap),  $\beta_C$  is the uncertainty in the capacity curve (e.g., 0.25 for high-code buildings), and  $\beta_T$  is the uncertainty in the damage state threshold (i.e., 0.4 for all building types (FEMA, 2020)). CONV() represents the convolution of demand and capacity uncertainties, which is needed because the reduced demand spectrum calculated in step 3 depends on the demand spectrum and the capacity curve. This convolution combines both the ground motion and structural uncertainty. However, it requires the combination of multiple non-symmetrical probability distributions, which increases the computational cost. Thus, Hazus assumes that  $\beta_D$  is constant throughout the analysis.

In contrast, this article argues that leaving  $\beta_D$  constant neglects important factors that affect the ground motion uncertainty. For example, it fails to take into account event-specific parameters such as seismometer density and other data sources, which update information about the location of the epicenter, acceleration magnitude, and rupture characteristics. The following section presents a methodology to overcome this assumption and include ground motion uncertainty information in Hazus damage assessment results.

*Integrating ground motion uncertainty: methods and results.* To modify  $\beta_D$  as new ShakeMap versions are published, a Monte Carlo simulation-based approach to obtain distributions of the building damage states is developed. This simulation allows for calculating the convolution of all random variables without the need for a closed mathematical form. Each simulation scenario requires the sampling of three random variables, which are lognormally distributed: the demand spectrum that comes from the ShakeMap (with  $\sigma = \beta_D$ ), the capacity curve that depends on the building (with  $\sigma = \beta_C$ ), and the damage state thresholds that depend on post-earthquake damage data (with  $\sigma = \beta_T$ ) (FEMA, 2020).

Taking the previously described four-step damage assessment process as a guide, the goal is to generate a distribution of the performance points leading to a distribution of estimated building damage states. This four-step process is the simplified version of the Hazus methodology, which uses expected spectral displacement and has ground motion uncertainty built into the fragility functions. Figure 7 depicts this process for a single version of the ShakeMap. The process consists of three main stages composed of five listed steps. First is a sampling stage (steps 1 and 2), where  $N$  samples of the demand spectrum and capacity curves are generated. These curves are sampled using Monte Carlo simulations, which use the distribution parameters of each ShakeMap version  $\beta_D$  and the building parameters and uncertainty  $\beta_C$ . The sampling process of the demand spectrum considers the correlation between  $PSA_{0.3}$  and  $PSA_{1.0}$  by sampling correlated lognormal realizations using the covariance published by Loth and Baker (2013, 2020). The resulting correlation has a value of 0.45. The resulting samples of  $PSA_{0.3}$  and  $PSA_{1.0}$  are then used to compute the demand spectra following the procedure presented in Section 5.6.1.2 of the Hazus earthquake technical manual (FEMA, 2020).

The second stage is a performance point stage (steps 3 and 4.1) where  $N$  performance points are found by merging the reduced demand spectrum and capacity curves. Then, using all  $N$  values of the performance point, a distribution of the points is computed. Third (steps 4.2 and 5), using the shape of this distribution and the damage thresholds  $\overline{S_{d,ds}}$  per damage state, a distribution of the five damage states (None, Slight, Moderate, Extensive, and Complete) is found.

Aside from the simulation of multiple random variables, the main difference between this methodology and the current Hazus methodology is step 4 in Figure 7. Fragility curves cannot be used in the proposed methodology as in the current Hazus methodology because these functions aggregate all the uncertainty from the variables into one probability distribution (see Equation 9). The existing method does not allow one to incorporate the evolution of ground motion uncertainty  $\beta_D$  as new information is collected. Instead, the proposed methodology generates Monte Carlo simulations of all the variables in the problem separately, allowing for the parameters of each variable to change with every ShakeMap version. Thus, in step 4.1 of the proposed methodology, all  $N$  simulated performance points are joined to build the three-dimensional (3D) histogram of the performance point distribution (step 4.1 in Figure 7). Then, in step 4.2, damage state thresholds are sampled knowing that they are lognormally distributed with parameters  $\overline{S_{d,ds}}$  and  $\beta_T$ , which depend on the damage state  $ds$  and the structural system of the building. For a given scenario  $i \in N$ , all four damage state thresholds are sampled (not including “None,” i.e.,  $S_d = 0$ ), and then, the probability of being at each damage state is found by integrating over the range of  $S_d$  and the sampled thresholds of consequent damage states (i.e., from  $S_{d,ds,i}$  to  $S_{d,ds+1,i}$ ) as in Equation 10.

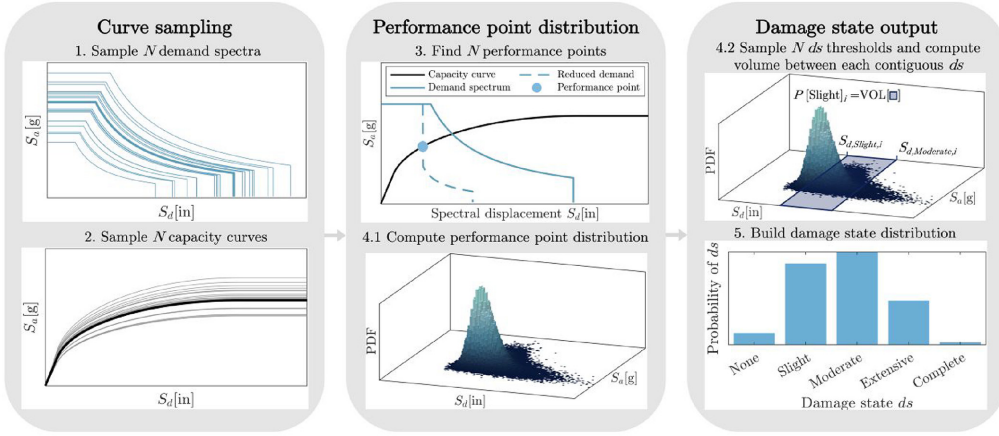


**Figure 7.** Simulation process for generating damage state probabilities.

$$P[ds]_i = \int_{S_{a,min}}^{S_{a,max}} \int_{S_{d,ds,i}}^{S_{d,ds+1,i}} PDF(\text{performance point}) \partial S_d \partial S_a \quad (10)$$

The integration is performed by finding the volume under the polygon of the performance point distribution and formed by the damage state  $ds$  and the next higher damage state (step 4.2 in Figure 7). Since the output of the simulation of the performance point PDF is discrete, the integral can be solved numerically by summing over the values of the PDF that fall between the limits in Equation 10.

A further step is needed to quantify damage state probabilities because the probabilities resulting from Equation 10 only account for one scenario  $i$ . Looking over multiple scenarios  $i \in N$ , the probability of being in each damage state is presented in Equation 11, which converges to the probability of being in each damage state when the number of samples  $N$  is sufficient (i.e., the variance of the distribution converges).

$$P[DS = ds] = \frac{\sum_{i \in N} P[ds]_i}{N} \quad (11)$$

To evaluate the impact of including ground motion uncertainty in Hazus damage assessment, the simulation procedure as shown in Figure 7 is implemented for both the Indios and Napa earthquakes, using all three locations of analysis (A, B, and C), and two versions of the ShakeMap: one before the FFM is added (version 1, called pre-FFM), and the other after FFM is included (version 8 in Indios, 27 in Napa, called post-FFM). The parameters used for the analysis are listed in Table 5. Structural system C1 represents a reinforced concrete moment-resisting frame. In total, 500,000 Monte Carlo simulations were used to generate the performance point distributions and damage state probabilities. The number of samples was validated using a variance convergence study, where the variance of  $S_d$  was monitored until it plateaus, that is, reaches convergence or the difference between the last five realizations is less than 0.1%. The convergence is required to confirm that the tails of the distribution are sufficiently sampled. The time required to run the simulation for a single building is 2.8 s, which demonstrates the usefulness of the proposed methodology for rapid damage assessment. In addition, parallel simulations can be used if



**Table 5.** Building parameters for Hazus methodology analysis

Parameter	Value
Structural system	C1
Height	Mid-rise
Fundamental period (s)	0.75
Code level	High code
Soil type	D

needed given that each realization is independent. An Apple M1 Pro processor was used to run the simulation process. Table 6 shows the results for all performance point distributions in the analysis.

To better visualize the differences between performance point distributions, Figure 8 shows the distributions for both events and ShakeMap versions at location B (coordinate at a cluster of low uncertainty near the epicenter). For the Indios earthquake, between the pre-FFM and post-FFM versions, there is a decrease both in the PGA and its uncertainty. As a result, the spectral displacement's standard deviation  $\sigma_{sd}$  decreases from 10.16 to 1.21 in, resulting in a narrower distribution post-FFM data compared with the distribution using information from the first ShakeMap version (see Figure 8a and c).

In comparison, for the Napa earthquake, even though the PGA uncertainty decreases in later versions of the ShakeMap (from 0.26(log g) at V1 to 0.11(log g) at V27), the distribution of the performance point is wider in the post-FFM version (see Figure 8b and d). This is due to the uncertainty in the capacity curve, which increases for larger values of ground displacement. For this case, the median PGA increased from 0.23 to 0.38 g from the pre-FFM to post-FFM versions. With the corresponding increase in capacity curve uncertainty, the convolution of the random variables results in a wider distribution for the performance points. Looking at the two events, the results emphasize the importance of considering each component of the uncertainty in the problem, including uncertainties in the capacity curve, damage state threshold, and ground motion parameters. In this case, accounting for the evolution of the ground motion uncertainty leads to changes in the uncertainties in both the capacity curve  $\beta_C$  and ground motion  $\beta_D$ .

Following the computation of performance point distributions, the damage state histograms are calculated according to the third stage of the process as shown in Figure 7. These histograms are shown in Figure 9 for the three locations of each event considered. Each subplot includes two histograms. First is the histogram using the methodology of implementing a dynamic ground motion uncertainty  $\beta_D$  (i.e., following the process proposed in Figure 7). Second is the histogram that results from using the current Hazus methodology, which changes the value of the ground motion median (i.e.,  $PGA_{med}$ ) with updated information from the ShakeMap, but not the ground motion uncertainty ( $\beta_D$ , which is equal to 0.5 regardless of the location or ShakeMap version).

The results in Figure 9 show the importance and impact of including dynamic ground motion uncertainty  $\beta_D$  in post-disaster building damage assessment. Changes in resulting damage state distributions across versions, in this case, pre- and post-FFM, are observed. Including the dynamic  $\beta_D$  results in either narrower or flatter damage state distributions depending on the event, specific location, or ShakeMap version. Across all cases, the average change of the probability of the damage state with maximum probability between

**Table 6.** Locations of analysis and parameters of performance point distributions

Event	Napa																							
	Indios				A				B				C											
Location	A				B				C				A				B				C			
Version	Pre-FFM	Post-FFM	Pre-FFM	Post-FFM	Pre-FFM	Post-FFM	Pre-FFM	Post-FFM	Pre-FFM	Post-FFM	Pre-FFM	Post-FFM	Pre-FFM	Post-FFM	Pre-FFM	Post-FFM	Pre-FFM	Post-FFM	Pre-FFM	Post-FFM	Pre-FFM	Post-FFM		
$PGA_{med} (g)$	0.32	0.58	0.29	0.24	0.13	0.15	0.14	0.15	0.13	0.15	0.14	0.15	0.13	0.15	0.14	0.15	0.13	0.15	0.14	0.15	0.13	0.15		
$\sigma_{PGA} (\beta_D)$	0.78	0.56	0.71	0.39	0.67	0.48	0.27	0.48	0.67	0.48	0.27	0.48	0.67	0.48	0.27	0.48	0.67	0.48	0.27	0.48	0.67	0.48		
$\bar{S}_d$ (in)	4.44	6.94	5.11	2.39	1.75	1.46	1.18	1.46	1.75	1.46	1.18	1.46	1.75	1.46	1.18	1.46	1.75	1.46	1.18	1.46	1.75	1.46		
$\sigma_{Sd}$	8.99	10.38	10.16	1.21	1.75	0.83	0.35	0.83	1.75	0.83	0.35	0.83	1.75	0.83	0.35	0.83	1.75	0.83	0.35	0.83	1.75	0.83		

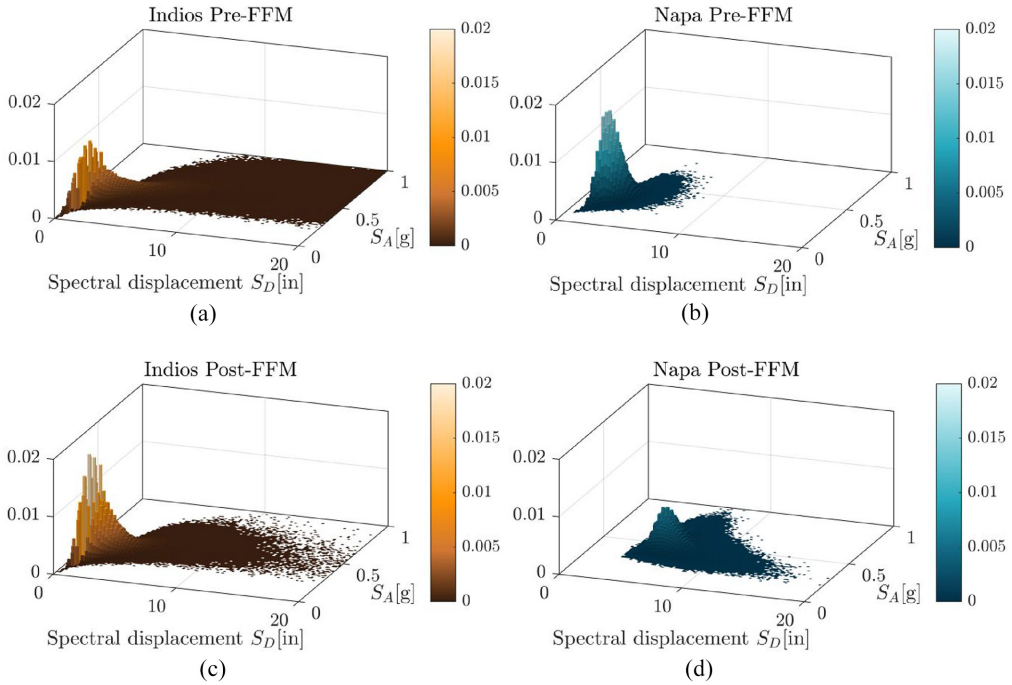


**Figure 8.** Performance point distributions for Indios ((a) and (c)) and Napa events ((b) and (d)) at location B.

using a dynamic compared with constant  $\beta_D$  is 13%. This number highlights the impact of considering evolving ground motion uncertainty in the analysis. Additional observations and examination of specific changes to the damage state distributions based on the results as shown in Figure 9 are as follows.

*Including dynamic  $\beta_D$  results in narrower distributions in most cases.* As a result, there is probability content more concentrated in a subset of the damage states, representing decreased uncertainty in the building damage assessment results. This effect can be seen in the results for the Indios earthquake at location C and for the Napa earthquake at locations A, B, and C. For example, at location B for the Napa earthquake pre-FFM, the dynamic  $\beta_D$  distribution is concentrated in the Slight damage state, with 0.18, 0.56, and 0.26 probability of being in the None, Slight, and Moderate damage states, respectively. In comparison, the constant  $\beta_D$  distribution is flatter (i.e., higher uncertainty), with 0.22, 0.37, and 0.37 probability in the same damage states.

*Large values of dynamic  $\beta_D$  can produce damage state distributions with higher uncertainty than using a constant  $\beta_D$ .* With pre-FFM information at locations A and B for the Indios earthquake, the distribution for the dynamic  $\beta_D$  is flatter compared with the constant  $\beta_D$ , indicating higher uncertainty in the distribution. This is not an error of the proposed methodology; instead, it is a more realistic and accurate representation of local properties, such as the lack of seismometers and information sources. Dynamic  $\beta_D$ , in this scenario, is 0.78 and 0.71 at each location, respectively, which is higher than the value used in Hazus

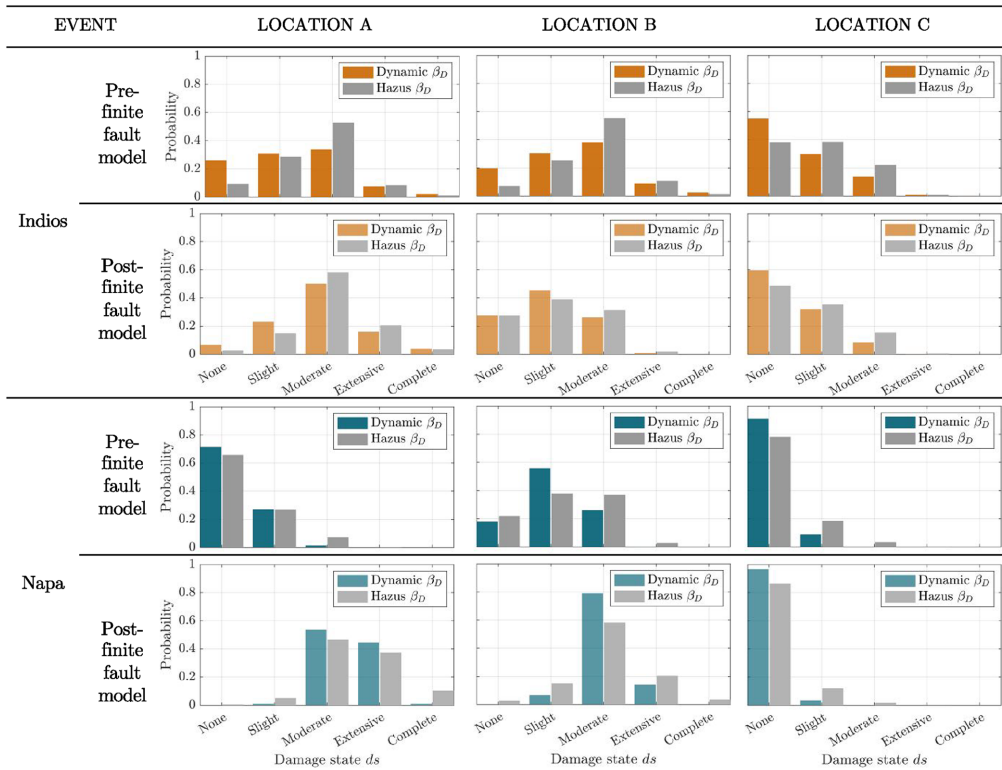


**Figure 9.** Damage state histograms for the Indios and Napa earthquakes. Each plot includes one histogram using a dynamic  $\beta_D$  as proposed in this study and the other using a constant  $\beta_D$  following the current Hazus methodology.

(0.5). These outcomes show the flexibility of the approach described in this article in incorporating ground motion uncertainty information to be able to accommodate data sources that are different for every event and location.

*Including a dynamic  $\beta_D$  can change the most probable damage state.* For example, this is evident at location A for the Indios earthquake. The pre-rupture estimation using a constant  $\beta_D$  results in a most likely Moderate damage state for the building, that is, the Moderate damage state has the highest probability among the five possible damage states. In comparison, incorporating the dynamic  $\beta_D$  results in a most likely damage state of Slight. This change can result in significant differences when calculating economic losses, as they typically do not scale linearly with damage states (Ramirez et al., 2012).

*When the value of dynamic  $\beta_D$  is similar to the constant  $\beta_D$ , the resulting damage state distribution is narrower.* Having a dynamic ground motion uncertainty means that a value of  $\beta_D$  can be close to the constant value used in Hazus (0.5). At location B for the Indios earthquake, for example, the dynamic  $\beta_D$  post-FFM is 0.48, which is close to the constant value used in Hazus (0.5). Therefore, the results should be similar. They are not the same, however, because properly convolving all random variables including dynamic ground motion

uncertainty  $\beta_D$  by following the proposed procedure in Figure 7 results in a treatment for damage state uncertainty that is more representative of actual event conditions, compared with the assumption made in Hazus, which uses a single lognormal function to account for all uncertainty sources in a damage state (see Equation 9). In fact, the values of dynamic  $\beta_D$  of the  $PSA_{0.3s}$  and  $PSA_{1s}$  are 0.59 and 0.58, respectively, meaning that there was larger uncertainty when building the demand spectrum than accounted for in the Hazus procedure with constant  $\beta_D$ . Even so, the resulting distribution using the dynamic  $\beta_D$  is narrower than that obtained using the existing Hazus approach. This example demonstrates that the current Hazus methodology is potentially overestimating the total uncertainty of damage states.

**The distribution of damage states between events is less variable for the Napa compared with Indios earthquake**, due to the increased data sources for ground motion parameter estimation leading to lower uncertainty values. Thus, there is less uncertainty in the outcomes than using the constant value used in Hazus. For instance, at location B for the Napa earthquake, both pre- and post-rupture histograms have more concentrated probability values compared with the results from using the constant  $\beta_D$ . The difference in uncertainty makes the post-FFM distribution include probability content in only three damage states, with the Moderate damage state accounting for 79% of the probability. On the contrary, the results from Hazus include probability content in all five damage states.

*The effects of dynamic  $\beta_D$  can also be appreciated in locations far from the epicenter, as in location C.* When comparing the distributions of both events, the variance of damages states in the Indios event is higher than in Napa, even when the values of PGA are relatively low and similar in both events. Note that the results between Hazus distributions in both events at location C are also different. This change results from the dependence of the effects on multiple pseudo-spectral accelerations (i.e.,  $PSA_{0.3s}$  and  $PSA_{1s}$ ) that are not reported in this article. Thus, while the PGA values for the case of location C post-rupture differ by 36% (0.15 g in Indios vs 0.11 g in Napa), the values of  $PSA_{1s}$  differ by 116% (0.11 g in Indios and 0.05 g in Napa).

As shown from the distributions' results, the inclusion of dynamic ground motion uncertainty more accurately represents the uncertainty that exists in estimating post-disaster building damage states and often results in narrower damage state distributions indicative of decreased uncertainty in damage assessment. It accounts for the full information that is available to characterize the ground motion, including evolution of the uncertainty in ground motion parameters in the time period after the event. In some cases, the shape and values of the damage state probability distributions significantly differ in using the dynamic compared with constant  $\beta_D$  value for ground motion uncertainty. In addition, the simulation approach for the random variables allows for capturing local properties such as the amount of information collected at different stages in the time period after the earthquake event. These improvements significantly impact economic assessments and all methodologies that depend on damage assessments, such as debris management, loss estimation, and population exposure.

In the case of estimating economic impacts of an earthquake, the results of these distributions are highly dependent on the distribution of damage states, given that the expected value of economic loss per building is calculated by multiplying the probability of being in each damage state by the expected repair/replacement cost of the building. Thus, even if

the damage state with the highest probability is the same between the proposed methodology and current Hazus calculations, it is the values of the probability of the building being in each damage state that is used to obtain the economic loss of the building. Varying probability content, as is found from using the dynamic compared with constant  $\beta_D$ , will result in different economic impact values. This consideration is especially relevant in the calculation of the cost of high-damage states, which grow exponentially and not linearly compared with the costs associated with lower-damage states (Ramirez et al., 2012). Thus, having a more accurate estimation of the uncertainty in building damage states can lead to improved economic loss distributions, both in terms of increased accuracy and lower uncertainty, which are crucial for an effective response to the earthquake.

### *Implementing the proposed approach for damage assessment*

The previous sections demonstrate that dynamic ground motion uncertainty can be successfully integrated into both the TZR and Hazus damage assessment methodologies. Both methodologies showed improved accuracy in the resulting damage distribution by incorporating the available information on ground motion hazard uncertainty, often resulting in narrower, that is, decreased uncertainty, distributions compared with the constant case.

To leverage the evolution of the ground motion uncertainty information available for use in post-earthquake damage assessment, the proposed methodology should be implemented multiple times as new versions of the ShakeMap are released after an event. Having an estimation of damage using the latest values of ground motion parameters is critical to achieving the highest accuracy and resolution of damage assessment possible when other detailed damage data are not available.

Given the input data required for each method, some limitations and comparisons should be considered when implementing the proposed methodology. In the case of the TZR model, the proposed procedure should be implemented when there is limited information about the building inventory and local properties. Incorporating the dynamic ground motion uncertainty allows for calculating different risk scenarios for post-disaster loss by using the updated beta distributions of the SEL. The resulting continuous distribution of SEL is useful when computing economic impacts at the aggregate level in large regions where building inventory data are not available. On the contrary, for the Hazus model, it is required to know detailed information about the building's structural system and the underlying soil characteristics to obtain accurate detailed results when combining these data with ground motion information. This information, however, is limited to the United States for Hazus. Thus, when implementing the proposed methodology, it is required to collect all necessary data to observe the benefit of including a dynamic ground motion uncertainty in the analysis.

## **Conclusion**

Detailed assessments of building damage after an earthquake are time and resource-intensive. Therefore, hazard-related data sets are highly valuable for estimating building damage in the immediate post-disaster period as these data sets are published within the first hours of the event. USGS's ShakeMap is one of these data sets, which provides detailed descriptions of ground motion parameters and their evolving uncertainties during the disaster response period. Information about the evolving ground motion uncertainty in earthquake parameters, however, has not been previously used in post-disaster building damage

assessment or incorporated into models of the total uncertainty in current damage assessment methodologies. Thus, this article combines the uncertainty evolution of seismic hazard parameters from USGS's ShakeMap with the earthquake loss methodologies from the revised TZR model and Hazus to evaluate the impact and demonstrate the need to incorporate dynamic ground motion uncertainty in damage assessment methodologies.

Using data from Puerto Rico's Indios earthquake in 2020 and the South Napa earthquake in 2014, it is first shown that ground motion uncertainty not only varies by event but also by location and time. For instance, for the Napa event, the estimated median PGA at the same location coordinate varied by up to 55% within the first 3 days of the earthquake. Similar changes in estimated PGA standard deviation were found. These changes have a significant impact on the resulting distributions of building damage states in the methodologies that depend on these ground motion parameters. Among the potential impacts are narrower distributions with probability content concentrated in fewer damage states, representing results with lower uncertainty and higher precision, and changes in the most probable damage state.

In the case of the TZR model, including ground motion uncertainty as a dynamic parameter results in improved estimation of exceedance probabilities of damage, resulting in narrower ranges for SEL estimates, which are widely used by financial entities for economic impact estimates in post-disaster contexts such as for insurance claims. The proposed inclusion of dynamic ground motion uncertainty also enables quantification of uncertainty in the results, usually represented by a variable that accounts for qualitative measures such as level of knowledge.

Compared with current Hazus methodologies, introducing dynamic uncertainty from the ShakeMap allows loss assessments to account for local features such as seismometer density, pre-existing knowledge of geology, and post-event collected data. The damage state distributions from Figure 9 show that including dynamic ground motion uncertainty can result in changes in the damage state of maximum probability. A comparison of the results of damage state distributions from the proposed methodology with those from the current Hazus methodology shows that Hazus potentially overestimates the total uncertainty in building damage by assuming a single probability distribution for all uncertainty sources. In addition, the average change of the damage state with maximum probability between the existing and proposed methodologies is 13%.

While most efforts to study uncertainty in building damage assessment have focused on modeling the structural response, this work focuses on improving the integration of the dynamic uncertainty of estimated ground motion parameters in damage assessment methodologies. This article does not consider damages from ground failures such as fault rupture, lateral spreading, liquefaction, or landslides given that the proposed methodology utilizes earthquake fragilities that depend on ground motion and not failure. Such studies can be the subject of future work. In addition, the sampling of random variables using Monte Carlo simulations in the proposed approach cannot be compounded for multiple locations, given the spatial correlation of the earthquake parameters. Further work can be conducted to improve the model to incorporate the spatial correlation and produce aggregate estimations of damage in a region.

## **Acknowledgments**

This work was supported by the Elizabeth and Bill Higginbotham Professorship for author Frost, and the Williams Family Professorship for author Tien is also acknowledged.


## Declaration of conflicting interests

The author(s) declared no potential conflicts of interest with respect to the research, authorship, and/or publication of this article.

## Funding

The author(s) disclosed receipt of the following financial support for the research, authorship, and/or publication of this article: This work was supported by the National Institute of Standards and Technology (Award #70NANB19H062).

## ORCID iDs

Jorge-Mario Lozano  <https://orcid.org/0000-0002-9219-3879>

Iris Tien  <https://orcid.org/0000-0002-1410-632X>

## Data and resources

This work did not produce new data to develop the proposed methodology. All data used for the methodology were properly cited throughout the manuscript.

## References

- Abrahamson NA and Bommer JJ (2005) Probability and uncertainty in seismic hazard analysis. *Earthquake Spectra* 21(2): 603–607.
- Abrahamson NA, Silva WJ and Kamai R (2014) Summary of the ASK14 ground motion relation for active crustal regions. *Earthquake Spectra*, 30(3): 1025–1055.
- Atkinson GM and Wald DJ (2007) “Did you feel It?” Intensity data: A surprisingly good measure of earthquake ground motion. *Seismological Research Letters* 78(3): 362–368.
- Baker JW, Bradley BA and Stafford PJ (2021) *Probabilistic Seismic Hazard and Risk Analysis*. Cambridge: Cambridge University Press.
- Bhattacharjee G, Soden R, Barns K, Loos S and Lallemand D (2022) Factors affecting earthquake responders’ building damage information needs and use. *Earthquake Spectra* 38(1): 56–80.
- Bommer JJ and Crowley H (2006) The influence of ground-motion variability in earthquake loss modelling. *Bulletin of Earthquake Engineering* 4(3): 231–248.
- Boore DM and Atkinson GM (2008) Ground-motion prediction equations for the average horizontal component of PGA, PGV, and 5%-damped PSA at spectral periods between 0.01s and 10.0s. *Earthquake Spectra*, 24(1): 99138.
- Boore DM, Stewart JP, Seyhan E and Atkinson GM (2014) NGA-West2 equations for predicting PGA, PGV, and 5% damped PSA for shallow crustal earthquakes. *Earthquake Spectra*, 30(3): 1057–1085.
- Campbell KW and Bozorgnia Y (2014) NGA-West2 ground motion model for the average horizontal components of PGA, PGV, and 5% damped linear acceleration response spectra. *Earthquake Spectra*, 30(3): 1087–1115.
- Borgonovo E, Zentner I, Pellegrini A, Tarantola S and de Rocquigny E (2013) On the importance of uncertain factors in seismic fragility assessment. *Reliability Engineering & System Safety* 109: 66–76.
- Celarec D and Dolšek M (2013) The impact of modelling uncertainties on the seismic performance assessment of reinforced concrete frame buildings. *Engineering Structures* 52: 340–354.
- Chiou BSJ and Youngs RR (2014) Update of the Chiou and Youngs NGA model for the average horizontal component of peak ground motion and response spectra. *Earthquake Spectra*, 30(3): 1117–1153.
- Doggett T and Fobert K (2013, May) Real-time catastrophe loss estimates—What do they really mean? Available at: <https://www.air-worldwide.com/publications/air-currents/2013/real-time-catastrophe-loss-estimates-what-do-they-really-mean/> (accessed 22 November 2023).



- FEMA. (2015). *Rapid Visual Screening of Buildings for Potential Seismic Hazards: Supporting Documentation*. Washington, DC: Government Printing Office.
- FEMA. (2020). *Hazus Earthquake Model Technical Manual*. Washington, DC: Government Printing Office.
- Handmer J (2002) The chimera of precision: Inherent uncertainties in disaster loss assessment. *International Journal of Mass Emergencies and Disasters* 20(3): 325–346.
- Ioannou I, Douglas J and Rossetto T (2015) Assessing the impact of ground-motion variability and uncertainty on empirical fragility curves. *Soil Dynamics and Earthquake Engineering* 69: 83–92.
- Kircher C (2002) Development of new fragility function betas for use with Shake Maps. *Unpublished Report, Palo Alto*. [https://scholar.google.com/co/scholar?hl=en&as\\_sdt=0%2C22&q=Kircher+C+%282002%29+Development+of+new+fragility+function+betas+for+use+with+Shake+Maps.+Unpublished+Report%2C+Palo+Alto&btnG=](https://scholar.google.com/co/scholar?hl=en&as_sdt=0%2C22&q=Kircher+C+%282002%29+Development+of+new+fragility+function+betas+for+use+with+Shake+Maps.+Unpublished+Report%2C+Palo+Alto&btnG=)
- Kircher CA, Whitman RV and Holmes WT (2006) HAZUS earthquake loss estimation methods. *Natural Hazards Review* 7(2): 45–59.
- Liel AB, Haselton CB, Deierlein GG and Baker JW (2009) Incorporating modeling uncertainties in the assessment of seismic collapse risk of buildings. *Structural Safety* 31(2): 197–211.
- Loth C and Baker JW (2013) A spatial cross-correlation model of spectral accelerations at multiple periods: Spatial cross-correlation of multiple-period spectral accelerations. *Earthquake Engineering & Structural Dynamics* 42(3): 397–417.
- Loth C and Baker JW (2020) Erratum: A spatial cross-correlation model for ground motion spectral accelerations at multiple periods. *Earthquake Engineering & Structural Dynamics* 49(3): 315–316.
- Porter K (2010) Cracking an open safe: Uncertainty in HAZUS-based seismic vulnerability functions. *Earthquake Spectra* 26(3): 893–900.
- Porter KA, Beck JL and Shaikhutdinov RV (2002) Sensitivity of building loss estimates to major uncertain variables. *Earthquake Spectra* 18(4): 719–743.
- Ramirez CM, Liel AB, Mitrani-Reiser J, Haselton CB, Spear AD, Steiner J, Deierlein GG and Miranda E (2012) Expected earthquake damage and repair costs in reinforced concrete frame buildings: Expected earthquake damage and repair costs in RC frame buildings. *Earthquake Engineering & Structural Dynamics* 41(11): 1455–1475.
- Rota M, Penna A and Magenes G (2014) A framework for the seismic assessment of existing masonry buildings accounting for different sources of uncertainty: Seismic assessment of masonry buildings accounting for uncertainty. *Earthquake Engineering & Structural Dynamics* 43(7): 1045–1066.
- Thiel CC and Zsutty TC (1987) Earthquake characteristics and damage statistics. *Earthquake Spectra* 3(4): 747–792.
- Thiel CC and Zsutty TC (2017) The Thiel–Zsutty earthquake damage model, reformulated and extended: TZR Reformulated and Extended- Part 1. *The Structural Design of Tall and Special Buildings* 26(7): e1348.
- US Geological Survey. (2014). M 6.0—South Napa. Available at: <https://earthquake.usgs.gov/earthquakes/eventpage/nc72282711/executive> (accessed 22 February 2022).
- US Geological Survey. (2020). M 6.4—13 km SSE of Maria Antonia, Puerto Rico. Available at: <https://earthquake.usgs.gov/earthquakes/eventpage/us70006vll/executive> (accessed 22 February 2022).
- Vamvatsikos D and Fragiadakis M (2009) Incremental dynamic analysis for estimating seismic performance sensitivity and uncertainty. *Earthquake Engineering & Structural Dynamics* 39: 141–163.
- Wald DJ, Lin K and Quitariano V (2008) *Quantifying and Qualifying USGS Shakemap Uncertainty*. Reston, VA: US Geological Survey.
- Wald DJ, Worden BC, Quitariano V and Pankow KL (2005) *Shakemap Manual: Technical Manual, User's Guide, and Software Guide* (Report 12-A1; Version 1.0, Techniques and Methods). Reston, VA: USGS Publications Warehouse.

- Wald DJ, Worden CB, Thompson EM and Hearne M (2022) ShakeMap operations, policies, and procedures. *Earthquake Spectra* 38(1): 756–777.
- Worden CB (2016) *Shakemap Manual* [Computer software]. Reston, VA: US Geological Survey.
- Worden CB, Thompson EM, Baker JW, Bradley BA, Luco N and Wald DJ (2018) Spatial and spectral interpolation of ground-motion intensity measure observations. *Bulletin of the Seismological Society of America* 108(2): 866–875.